United States Air Force
Research Laboratory

RADIO FREQUENCY DOSIMETRY AT THE AIR FORCE RESEARCH LABORATORY

William Hurt

Leland Johnson

Charles Kuhnel

HUMAN EFFECTIVENESS DIRECTORATE
DIRECTED ENERGY BIOEFFECTS DIVISION
RADIOFREQUENCY RADIATION BRANCH
8262 HAWKS ROAD
BROOKS CITY-BASE TX 78235-5147

January 2004

20040303 296

NOTICES

This report is published in the interest of scientific and technical information exchange and does not constitute approval or disapproval of its ideas or findings.

This report is published as received and has not been edited by the publication staff of the Air Force Research Laboratory.

Using Government drawings, specifications, or other data included in this document for any purpose other than Government-related procurement does not in any way obligate the US Government. The fact that the Government formulated or supplied the drawings, specifications, or other data, does not license the holder or any other person or corporation, or convey any rights or permission to manufacture, use, or sell any patented invention that may relate to them.

The Office of Public Affairs has reviewed this paper, and it is releasable to the National Technical Information Service, where it will be available to the general public, including foreign nationals.

This report has been reviewed and is approved for publication.

//SIGNED//

WILLIAM D. HURT
Senior Physicist

//SIGNED//

GARRETT D. POLHAMUS, DR-IV (GM-15), DAF
Chief, Directed Energy Bioeffects Division

REPORT DOCUMENTATION PAGE

1. REPORT DATE (DD-MM-YYYY)	2. REPORT TYPE	3. DATES COVERED (From - To)
December 2003	Final	01-10-1997 to 31-12-2003

4. TITLE AND SUBTITLE	5a. CONTRACT NUMBER
Radio Frequency Dosimetry at the Air Force Research Laboratory	
	5b. GRANT NUMBER
	5c. PROGRAM ELEMENT NUMBER
	62202F

6. AUTHOR(S)	5d. PROJECT NUMBER
William D. Hurt, Leland R. Johnson, Charles T. Kuhnel	7757
	5e. TASK NUMBER
	B3
	5f. WORK UNIT NUMBER
	31

7. PERFORMING ORGANIZATION NAME(S) AND ADDRESS(ES)	8. PERFORMING ORGANIZATION REPORT NUMBER
Human Effectiveness Directorate Directed Energy Bioeffects Division Radio Frequency Radiation Branch 8262 Hawks Road Brooks City-Base, TX 78235-5147	

9. SPONSORING / MONITORING AGENCY NAME(S) AND ADDRESS(ES)	10. SPONSOR/MONITOR'S ACRONYM(S)
Human Effectiveness Directorate Directed Energy Bioeffects Division	AFRL/HE
Radio Frequency Radiation Branch 8262 Hawks Road Brooks City-Base, TX 78235-5147	11. SPONSOR/MONITOR'S REPORT NUMBER(S) AFRL-HE-BR-TR-2003-0162

12. DISTRIBUTION / AVAILABILITY STATEMENT
Approved for public release, distribution unlimited.

13. SUPPLEMENTARY NOTES

14. ABSTRACT
Knowledge of internal E- and H-fields, induced current densities, and SARs is of basic interest in the assessment of biological effects and medical applications of electromagnetic fields. Dosimetry is an important part of any scientific effort to assess the effects of EMF on biological organisms. Experimental dosimetry is essential in determining the internal fields and the whole body or localized SAR values in experiments with phantoms or animals. Carefully performed experiments are crucial in verification of theoretical predictions. In the last few years, considerable progress has been achieved in experimental and numerical dosimetry. Today a broad range of tools for dosimetric analysis for the wide frequency range is available. Because of the heterogeneity of the tissues and the nonuniformity of the incident fields, closed form analytical solutions are impossible and computer methods are needed to obtain the internally coupled fields. In theoretical dosimetry, FDTD is currently the most acceptable choice if digital anatomical models of man and animals are to be analyzed. The main contribution of our research efforts to the discipline of theoretical dosimetry is identification of the dependence of predicted SAR in relation to the variability in permittivity values for different tissue types when using different numerical anatomical models.

15. SUBJECT TERMS
Bioeffects, Radiofrequency Radiation, Specific Absorption Rate

16. SECURITY CLASSIFICATION OF:			17. LIMITATION OF ABSTRACT	18. NUMBER OF PAGES	19a. NAME OF RESPONSIBLE PERSON
			Unclass	29	William Hurt
a. REPORT	b. ABSTRACT	c. THIS PAGE			19b. TELEPHONE NUMBER (include area code)
Unclass	Unclass	Unclass			(210) 536-3167

TABLE OF CONTENTS

FIGURES

TABLES

1.0 **INTRODUCTION**

In the last three decades, the use of devices that emit radio frequency (RF) fields has increased dramatically. The proliferation of RF devices has been accompanied by increased concern about ensuring the safety of their use. Throughout the world many organizations, both government and non-government, have established RF safety standards or guidelines for exposure. Because of different safety philosophies, the former USSR and some of the Eastern European countries have more stringent safety standards than most Western countries. The maximum permissible exposure in some Eastern European and Western countries differ by over two orders of magnitude. These differences have raised concerns about the lack of uniformity and have led to public concern and distrust about electromagnetic fields (EMF) exposures in controlled and uncontrolled environments[1]. One concern about these differences is interpretation of data from animal studies. Can the effects observed in animals exposed to EMFs be used to set human exposure standards? Which effects are important for human safety and which are not? In applying safety standards the issue of how to measure EMF absorption in the body is not easily solved. Typically, what is specified in the safety standard is field strength or power density that should not be exceeded. These limits are designed to prevent excessively high specific absorption rates (SAR) in the human body. Thus, better methods are needed to properly measure EMF absorption and, extrapolate or relate effects observed in animals to those expected to be found in people. The resulting data could lead to modification of existing safety standards or establishment of new safety standards.

Accurate dosimetry represents an essential element of the research in determining the biological effects of EMF. Electromagnetic energy is absorbed non-uniformly in biological tissues[2-4]. A large number of factors such as a body's shape and position, as well as its orientation in the field influence these non-uniform distributions[5,6]. In short, there is no single answer to the question, "How much electromagnetic field energy will be absorbed?". In order to ensure the safe use of EMF emitting devices, a number of techniques for measuring EMF exposure have been developed, however, they all have limitations. Since the energy absorbed is directly related to the internal EMF (that is, the EMF inside the object, not the EMF incident upon the object), dosimetry is also interpreted as the determination of internal EM fields. First, we need dosimetry to determine which internal fields in animals cause a given biological effect. Then we need dosimetry to determine which incident fields would produce similar internal fields in people, and therefore a similar biological effect. Dosimetry is needed whether the effects are produced by low-level internal fields or by more intense fields that cause body temperature to rise. Since internal and incident EMF can be quite different, depending on the size and shape of the object, its electrical properties, its orientation with respect to the incident EMF, and the frequency of the incident fields[7], the development of theoretical dosimetry modeling techniques and powerful computer hardware has resulted in dosimetry modeling as a principle tool in determining EMF exposure.

The results of the output from any model, including Finite-Difference Time-Domain (FDTD), are questionable if the model has not been validated with empirical data. Validation is the key issue in earning the credibility of advanced theoretical modeling and offers a unique bridge between theoretical and experimental dosimetry.

Since applied methods in experimental dosimetry require the implantation of thermal or E-field probes into deep body organs, it is not feasible to perform such studies in human subjects, therefore validation attempts of the computer models must be accomplished using phantoms (simplistic geometry and tissue equivalent materials) and laboratory animals. Good correlation between the predicted and empirical phantom and animal data would provide increased confidence in the results predicted by the man model[8]. A simplistic phantom composed of a sphere is a useful and convenient method to validate FDTD predictions of the SAR values[9-12]. In addition, the Mie solution[13], which provides an exact value for spheres, can be used to measure error in both empirical data and FDTD data. Many sophisticated, high-resolution digital anatomical models that are being developed call for validation that employs not only simplistic geometry models, but also the actual type of organisms used to develop these models. The brain of the rat offers an ideal organ for comparison, due to the precision of stereotaxic probe placement, as well as the ability to easily confirm probe placements in tissue sections following experimentation[14].

The facilities at the Radiofrequency Radiation Branch (HEDR), Air Force Research Laboratory, for accomplishing these empirical measurements are described below.

2.0 <u>EXPERIMENTAL</u> <u>DOSIMETRY</u>

Measurements of the external fields for the evaluation of exposure conditions are usually considered a part of experimental dosimetry. To place the measurements of external fields vs. internal fields in proper perspective, one must realize that the instruments and methods for measurements of internal fields are not suitable for use on humans except in hyperthermic treatment for cancer therapy[15]. Therefore, to prevent potentially hazardous exposures to humans, the external fields are measured. Data on the intensities of external fields that potentially constitute a hazard to man are obtained through experimental evaluation of the intensities of the internal fields and the resulting SAR in animals and determination of external fields which produce similar internal fields (SAR) in man.

2.1 Exposure Facilities

During many radio frequency (RF) exposures, it is important to know the incident power density. There are many means of determining this power density. The three most common used are a RF survey meter in conjunction with a compatible probe, a calibrated power sensor and an antenna with a well defined capture area, and temperature differences (ΔT) measurements using an infrared camera and carbon-loaded Teflon (See Tables 1-3 and Fig. 1-5). For the frequency range of 30 kHz to 40 GHz, the favorite method is using the RF survey equipment.

There are a few manufacturers of RF survey equipment. Narda Microwave manufactures the primary instrument used to measure electromagnetic fields. The two meters used are the 8617 analog meter with appropriate probe or the 8718 digital meter. Using either meter is relatively easy. The probe and meter are calibrated together and

zeroed in a zero field environment. The probe is then placed in the RF field to be measured. The probes are isotropic, but the best practice is to face the probe head toward the RF source. There are three elements in the probe head, so in order to best align the elements, the probe is rotated through $360°$ and measurements recorded every $45°$. These numbers are then averaged and the standard deviation is calculated. Next, add the standard deviation to the average and apply the correction factor for the probe. Using a spreadsheet makes the calculations very quick and easy. For lower and higher frequency fields, other techniques were developed.

Millimeter waves are not easily measured using the RF survey equipment. A method using a power sensor and a capture device was developed. A combination of an HP/Agilent W8486A waveguide power sensor and Millitech standard gain pyramidal horn connected to an Agilent 437B power meter is used to measure the fields from 75 – 110 GHz. The USAF Precision Measurements Equipment Laboratory (PMEL) calibrates both the power sensor and power meter. The effective area (A_e) of the horn is determined from the actual gain of the horn. For very small spot sizes, an open-ended waveguide section can be used in lieu of a horn. The A_e however, is not easy to determine. The only reliable method of determining the correction factor is to do a side-by-side comparison with a known measurement device. The open-ended waveguide is very frequency and angle sensitive. Attenuators can be placed in line after the horn to extend the useful power measurement range. For very high power densities, other methods must be used.

Numerous materials were investigated as tools to over come the restriction of power density or spot size. These materials were looked at with an infrared camera to measure temperature rise verse power density. RF cloth or carbon-impregnated cloth was first tried. This material responds to RF exposure with a very uniform temperature rise, but with no significant thermal mass, it was very susceptible to environmental conditions. Carbon loaded Teflon was tried next. This material has very uniform characteristics and has enough mass to be minimally effected by environmental conditions. Extensive temperature rise measurements using an infrared camera were performed in an environmentally controlled chamber. Power density was measured using the waveguide sensor described earlier. A series of points were generated and an equation developed to correlate the temperature rise with power density. The carbon-loaded Teflon is also very useful in mapping fields that have interference patterns. The maximum and minimum points are easily determined. From the interference patterns, the average delivered power can be calculated. Other uses for carbon-loaded Teflon are still being investigated. More accurate and defined calibration procedures are being developed. With time, this technique should prove very useful.

These are only a few types of measurements that can be made. Dipole antennas and H-field loops are some other common methods that have been used[16]. Other techniques may allow us to make more accurate measurements.

All power measurement equipment and blackbody source calibration is performed by or certified by PMEL located at Brooks City-Base under the 311 Mission Support Group/Logistics (311MSG/LG).

3

Table 1. RF Measurement Resources

RESOURCE	MAKE	MODEL	RANGE	ACCURACY
RF Power Meter	Hewlett Packard	HP437B	Determined By Probe Used	Absolute Mode +/- .02dB or +/-.5 %
RF Power Meter	Narda	8718	Determined By Probe Used	Determined By Probe Used
RF Power Sensor	Hewlett Packard	W8486A	75 GHz to 110 GHz	Power Linearity ±□
RF Power Sensor	Hewlett Packard	R8486A	26.5 GHz to 40 GHz	Power Linearity: ±3%
RF Power Probe	Narda	8723	300MHz to 50GHz	+1.25/-3.0 dB (0.3 GHz to 50 GHz) ± 1.25 dB (1 GHz to 50 GHz)
RF Power Probe	Narda	8762	300KHz to 1GHz	± dB(3 MHz to 300 MHz) ±2 dB (300 kHz to 1 GHz)
Standard Gain Horn	Millitech	SGH-10-RP000	75-110GHz	Gain=23.2 db @ 93.2 GHz
Waveguide Attenuator	Dorado	FA10-10	75-110GHz	±1.5db
IR Camera	Flir	ThermaCAM® S60	-40°C -1500 °C	±2°C or ±2%
IR Camera	Flir	ThermaCAM® SC 3000	-20°C to 1500°C	± 1°C or ± 1%
IR Camera	Indigo	Merlin Mid	0 to 350°C	± 2 °C or ± 2%
IR Camera	Amber	Radiance-1 Thermographic	Determined By Black Body Cal.	Determined By Black Body Cal.
Open-ended Waveguide	Fabricated In-house	N/A	75-110GHz	Determined By Comparison
Blackbody Source	Mikron	340	-20 to 150°C	± .3°C
Blackbody Source	Mikron	345X8	-10.00 to 148.9°C	≤ 20mk

Table 2. Available Exposure Systems

| Freq (MHz)	Avg Power (W)	Peak Power (W)	Bldg	Room/ Chamber	Manufacture	Comments
10-220	2k	CW	1161	Ch 1	Amplifer Research	dipole antennas
50 – 200	2k	CW	1161	Ch 1	Southwest Research Institute	Solid State
95000	750	3k	1161	Ch 2	Polarity Inc	Delivery cy 2004
915	75k	CW	1162	1130	Microdry	
2450	1k	CW	1162		Cober	Portable
2450	1k	CW	1162		MCL	Portable
35000	75	CW	1162	1133	Applied Elecromagnetics	Dual Freq Cabinet
95000	50	CW	1162	1133	Applied Elecromagnetics	Dual Freq Cabinet
95000	100	CW	1162	1125	CPI	
UWB			1162	1077	Various	
750 – 975	3k	CW	1183	Ch 9	MRC-113	Removed from Van
2070	10k	CW	1183	Ch 8	Cober	
8300	20k	CW	1183	Ch 9	Cober	
35000	750	3500	1183	Ch 7	General Electric	Scheduled for DRMO
2070	20k	CW	1185	Ch 3	Cober	Part of PPES
2800	2k	2M	1185	Ch 3	Cober	Part of PPES
5600	1k	1M	1185	Ch 3 / Ch 4	Cober	Part of PPES
93000	700	700k	1185	Ch 3	Cober	Part of PPES
94000	800	4k	1185	Ch 3	Northstar	
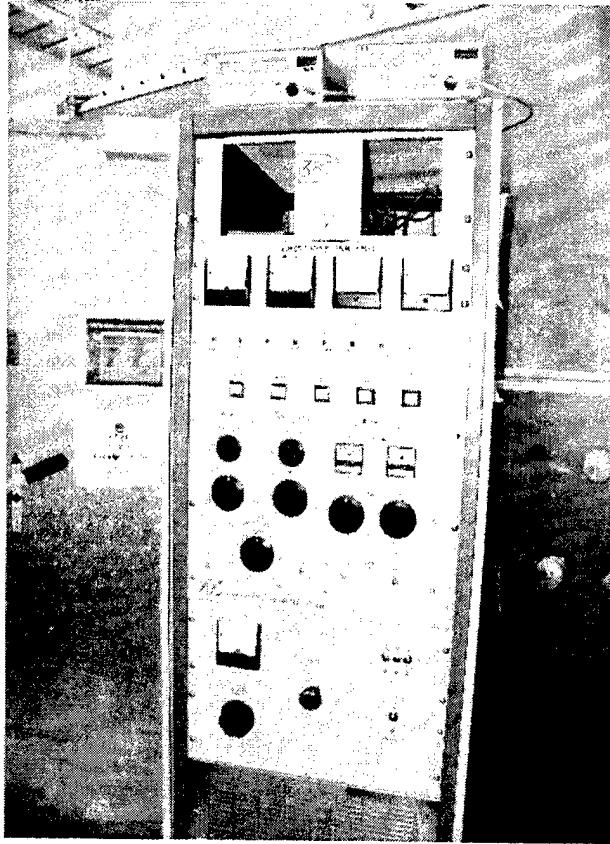
Figure 1. Applied Elecromagnetics 35/94 GHz System.
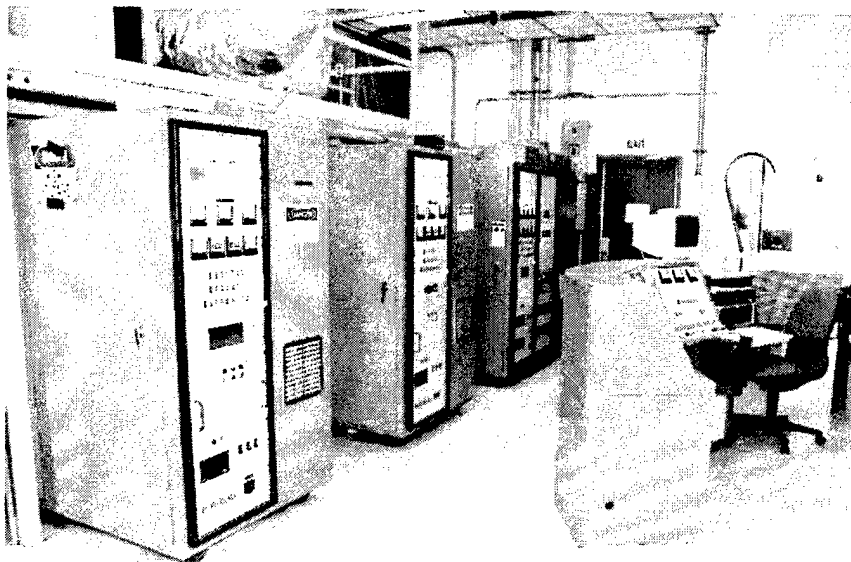
Figure 2. Peak Power Emission System (PPES).

Table 3. Available Chambers

Chamber #	Bldg	Rm	Dimension External w x l x h (ft)	Dimension Internal w x l x h (ft)	Frequency	Environmental Control
1	1161		22 x 32 x 22	10 x 20 x 10	> 50 MHz	18-30°C ±0.5°C
2	1161		12 x 20 x 10	10 x 18 x 9	> 1 GHz	15-30°C ±1.0°C
3	1185		24 x 40 x 10	22 x 38 x 9	> 1 GHz	10-35°C ±1.0°C Hum 30-95%
4	1185		8 x 12 x 8	6 x 10 x 6	> 1 GHz	18-30°C ±0.5°C
5	Mobile Trailer		10 x 14 x 8	8 x 12 x 6	> 1 GHz	10-35°C ±0.5°C
7	1183		12 x 16 x 10	11 x 15 x 9	>10 GHz	10-35°C ±0.5°C
8	1183		14 x 24 x 10	12 x 22 x 8	> 1 GHz	10-35°C ±0.5°C
9	1183		14 x 24 x 10	12 x 22 x 8	> 1 GHz	10-35°C ±0.5°C
10	1162	1125	12 x 16 x 12	10 x 14 x 10	> 1 GHz	15-30°C ±1.0°C
11	1162	1130	20 x 24 x 10	20 x 24 x 10		None
12	1162	1133	8 x 10 x 8	7 x 9 x 7	> 1 GHz	15-30°C ±1.0°C
Circular Waveguide	1162	1132	12 x 24 x 9			Building 100% fresh air
Acoustic	1162	1133				Building

Figure 3. Chamber 1 in Bldg. 1161 with MHz dipole and corner reflector antenna.
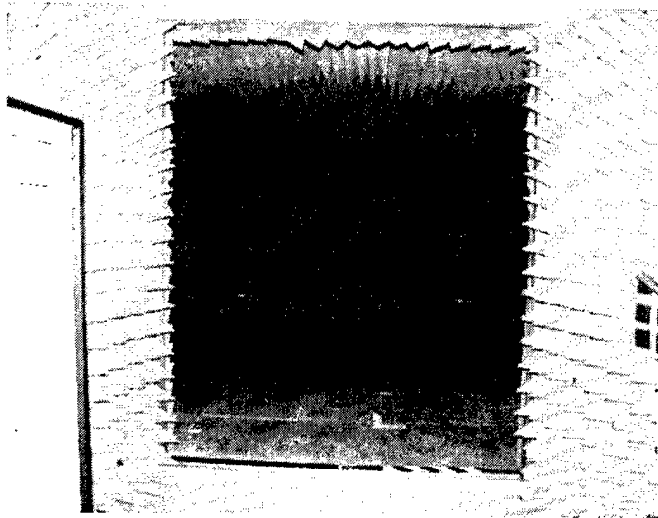
Figure 4. Chamber 8 in Bldg. 1183.

RF Chambers & Transmitters

1183

9- 740-980 MHz, 6kW
9- 8.3 GHz, 20kW
8- 2.07 GHz, 10kW
7- 35 GHz, 800W

9 - 24 x 14 x 10
8 - 24 x 14 x 10
7 - 12 x 16 x 10

5 - 10 x 14 x 8

Mobile Lab

1185

4 - 8 x 12 x 8

3 - 24 x 40 x 10

3- 9.3-9.4 GHz, 1kW
3- 5.4-5.8 GHz, 1kW
3 – 2.8GHz, 2kW
3- 2.07 GHz, 20kW
3- 94 GHz, 500W

10 – 12 x 16 x 12
11 - 18 x 20 x 10
12 – 8 x 10 x 8
CWG - 12 x 24
UWB - 14 x 16

10 - 95GHz, 100W
11 - 915MHz, 75kW
12 - 35/94 GHz, 50W
14 - UWB

1162

Note:
UWB - Ultra-wideband
CWG - Circular waveguide

Support area includes:
 Transmitters
 Experimental equipment
 Spare parts

1 - 22 x 32 x 22
2 – 12 x 20 x 10

1161

1 - VHF, 50-200MHz, 2kW
1 – 10 - 220 MHz, 2kW
2 – 95 GHz, 800W (cy2004)
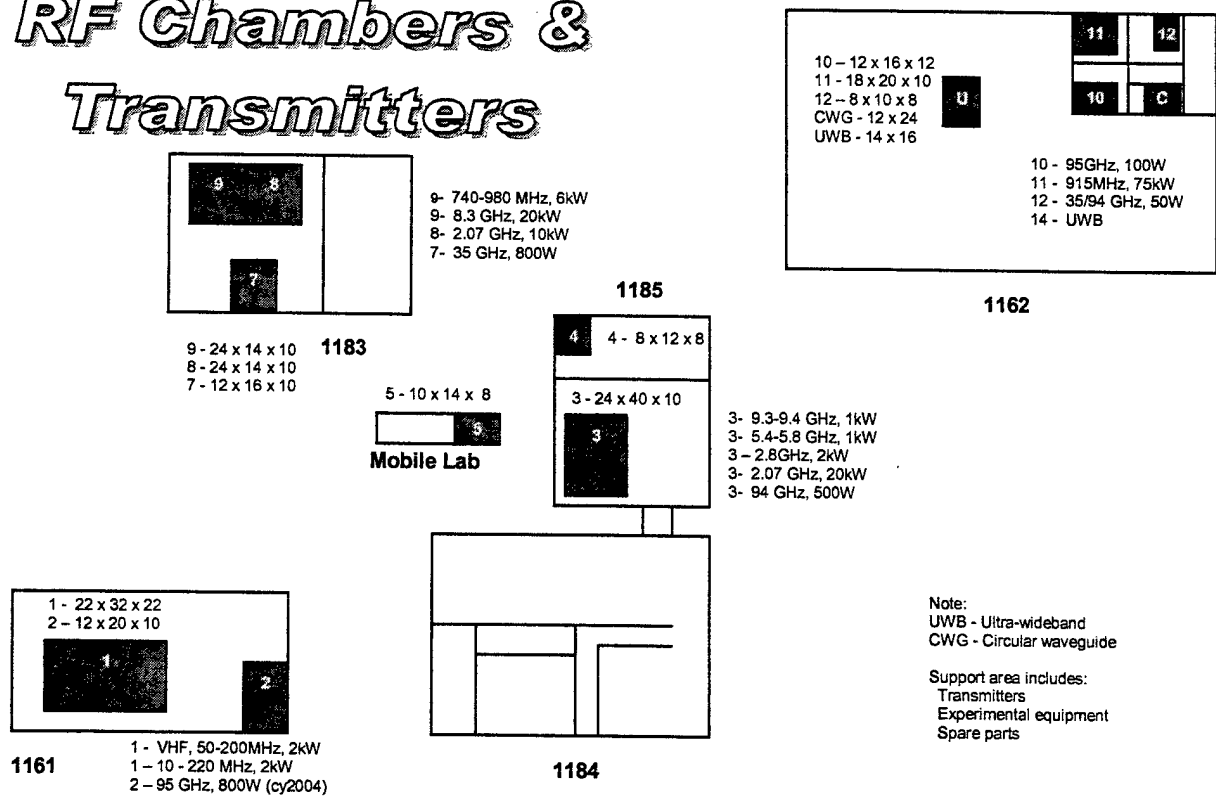
1184

Figure 5. Map of HEDR Compound.

2.2 Measuring SAR

Experimental dosimetry includes the following areas: measurements of total SAR and its distribution in live or dead experimental animals, measurements of average SAR and SAR distribution in models of animals and humans (phantoms), and development of exposure devices for animals and *in vitro* preparations in which quantification of exposure conditions and internal fields is facilitated[17]. Experimental dosimetry plays a crucial role in the control of animal exposures and quantification of the data from animal experimentation. It enables comparison of experiments conducted in various laboratories, under different exposure conditions, and for different species. It also plays an important role in validation of the calculations from theoretical dosimetry. The dosimetric data can be used to extrapolate the results of animal experiments to human exposures where the physical scaling principle is employed[5]. Generally, accepted methods of measurement of SAR include measurement of the rate of temperature rise within the exposed object or measurement of the internal E-field strength. Temperature rise may be characterized by a whole-body-averaged (calorimetric) measurement, a point measurement (via a thermometer implanted in the body being exposed), or infrared thermographic camera analysis of bisected phantom models that have been exposed to large RF fields[18]. The internal electric field strength may be measured by an implantable E-field probe[19].

2.3 Temperature Measurement Techniques

An important advantage of the temperature measurement technique is that temperature is a scalar value, making it easier to produce probes of very small size having short time constants[5]. One major difficulty is the need for high power RF sources in order to achieve large enough SAR values for accurate measurement, i.e. < 1 W/kg. Another important drawback is that the time derivative can only be determined by temperature measurements at two discrete times, whereby the thermodynamic state prior to exposure must be known and should preferably be in equilibrium[19]. Since the exposure alters thermal equilibrium, means must be provided to re-establish equilibrium after each measurement cycle, which is usually time consuming.

Average whole body SAR may be measured using calorimetric methods. Such methods have been used predominantly with small animals or animal models[3,20,21], but also to measure SAR in a full-size human model[22]. Although the calorimetric determination of the energy stored in the model once inside the calorimeter is quite accurate per se, the overall system accuracy in terms of SAR is limited by how closely the test object models the actual object and by the amount of irradiation-induced heat that escapes from the object that is not measured. This method, moreover, requires sufficient time for the thermal equilibration processes to occur and requires sufficient energy deposition in the test object to produce a calorimeter output signal that is enough above baseline to be measurable.

However, the Dewar-flask method of calorimetry is a relatively straightforward way of determining the whole-body average SAR of small-bodied animals[21,23]. The calorimetric technique of determining a whole-body average temperature requires that the cadaver be immersed in a Dewar flask containing a medium, such as water, at a

known temperature; then the temperature of the carcass, following irradiation, can be determined by calculating the final temperature of the carcass.

Non-perturbing temperature probes (small, high resistance thermistors with high resistance leads) can be used successfully to make SAR measurements especially point measurements in very small structures (e.g. small locations in animal's brain). The minimum requirements are that the temperature sensor and associated leads should be nonperturbing to the EMF, and the SAR should be large enough to produce a measurable temperature rise during a period of about 30 seconds. The first requirement can be satisfied by using highly resistive material or fiber optics, instead of metal components, for the temperature-sensing element leads[24]. The second requirement entails the measurement of SARs no lower than a few W/kg. This lower limit exists because the resolution of most temperature probes is typically 0.01 to 0.1°C, and the longest practical duration of irradiation that allows reasonably accurate SAR measurement is typically between 20 and 30 seconds[14] because longer exposures allow heat loss to occur.

Our instrument of choice is an in-house developed temperature measurement and acquisition system (TMAS)(See Fig. 6 and Table 4). It was designed around the BSD non-perturbing thermister probe developed by Ronald R. Bowman[25]. In addition to the BSD probe, the system consists of an 8-channel interface box[26], a National Instruments acquisition card, and LabVIEW based software run on a notebook computer.

The interface consists of a highly stable precision constant current source providing excitation for the thermister. The voltage developed across the thermister is fed into a very high impedance instrumentation amplifier. The signal is scaled to match the A-D card and then low-pass filtered at 10 Hz. This signal is then cabled to the A-D card located in the computer. The front panel provides input jacks for the probes and a power LED. The rear panel contains the On/Off switch power connector and an output connector. The interface is powered by common 120VAC.

The Software was developed using the Graphical programming language LabView. It quantatizes the interface outputs at 400 samples/sec, averaging 80 samples 5 times/sec. This provides 5 data points/sec max, which is based on the time constant of the probe. The software linearizes the thermister output using the Steinhart and Hart[70] equation for thermisters. Coefficients for the equation are derived during the calibration process. The software provides spreadsheet compatible data that includes date, time and sample number from start for each data point. The computer display provides all operational controls, data/file/path display and real-time charting.

A thermographic camera can be used to measure temperatures and ultimately SAR across the visible surface of an object[18, 27]. Since the camera is non-invasive it can be used in addition to other measurement techniques. The method involves the use of a radiometric camera for recording the rate of rise of temperature in a plane that bisects an entire model (phantom) or a cadaver of a biological subject under study. The temperature distribution before, and immediately after brief, high-power irradiation, is observed on the precut surface on each half of the bisected model. This is done to prevent cooling by evaporation or flow of the wet synthetic tissue out of its shell (usually composed of synthetic fat or rigid plastic foam). This procedure is also used to measure heating patterns on the surface of subjects exposed to RF fields[28]. Infrared thermometry offers at least three advantages: 1) temperature measurements are recorded in real time, by a system with fast effective response time, thus eliminating any temporal error due to the

10

finite response time of thermistors or thermocouples, 2) the sensor array of the IR camera allows the simultaneous sampling of multiple discrete areas, and (3) no sensor is placed in contact with the tissue, which reduces the chance of artifact. This latter advantage assures that measurements are obtained from the site that reaches the maximal temperature, thus eliminating error due to less-than-optimal placement of a single probe.
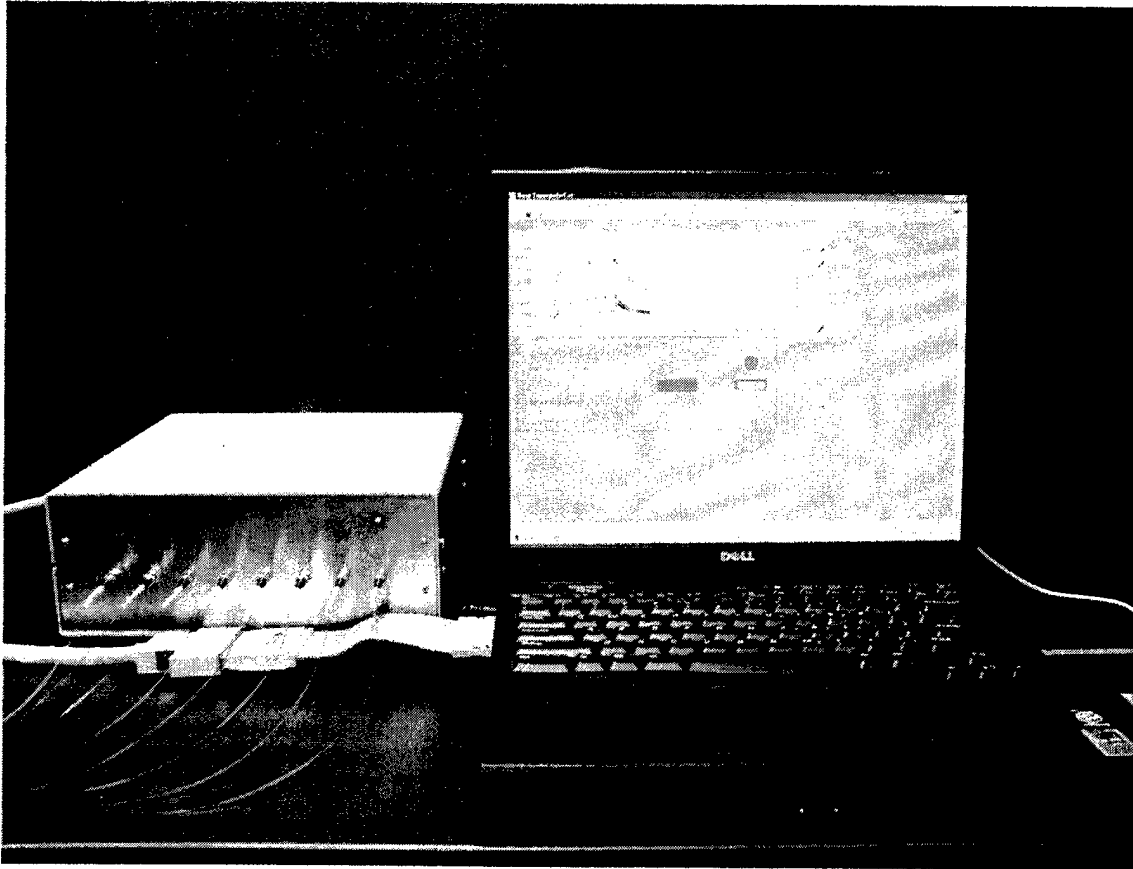

Figure 6. Temperature measurement and acquisition system (TMAS).

Table 4. HEDR TMAS Specifications

Accuracy:	0.1deg C
Resolution:	0.01deg C
Stability:	+/-. 05deg C, Tested to one month
Channels:	8
Range:	18-60deg C
Software:	LabVIEW Custom Application
Power:	120VAC

2.4 Electric Field Measurement Techniques

Since thermal as well as non-thermal interactions of RF fields with organisms are related to the internal E-field intensity, E-field sensors have been developed[29]. In fact, the simplest way of measuring electric field is to use a monopole or dipole antenna at the end of coaxial line that is connected to a detection and measuring system.

Miniature isotropic, three-dimensional diode-loaded E-field probes with high impedance feed lines, which have been commercially available for a number of years, have been used to measure SAR distributions in phantom models and in living, anesthetized animals[30]. This type of probe can be inserted into a sample in the same manner as the non-perturbing temperature probes. These probes measure the intensity of the internal E-field at the location of the probe.

2.5 Power Difference Method

Whole-body dosimetry may be performed using a Power Difference method that is limited to closed exposure systems such as waveguides, TEM-mode transmission lines, cavities, *etc.* In this method, power meters are attached to the exposure systems by directional couplers to measure the incident, reflected, and transmitted power. The power absorbed by the biological target (whole-body absorption rate) is then measured by subtracting the values of the reflected and transmitted power from the incident power. For exposure systems using live animals, the values of these three measurements vary as the animals change position and posture because absorption is a function of the animal's orientation relative to the field polarizations. It is thus desirable to have a data collection system that can integrate the measured power difference and determine a temporal average, usually for the duration of exposure.[31, 32] The advantage of this method is that it is capable of providing on-line instantaneous measurements of the whole-body absorption rate in live animals. As such, the method is useful for continuously monitoring absorption changes created by alterations in an animal's position, posture, *etc.* There are, however, some problems. In cases involving a multiple-animal exposure within the same closed system, the measured absorption rate represents the sum total for all animals. How this energy is distributed among the animals within the system cannot be determined. The method is, however, optimal for single-animal exposures.

3.0 SAR MODELING

The last decade has witnessed significant progress in numerical dosimetry for human exposure to RF fields. With the development of the FDTD method, it is possible to predict electric field strength and SAR values in various biological tissues under a wide range of exposure conditions in phantoms and laboratory animals, as well as humans. Permittivity values play a dominant role in the overall consideration of interaction between EMF and matter and in related applications including EM dosimetry.

The rigorous analysis of a realistically shaped heterogeneous model for humans or experimental animals is a difficult theoretical task. Because of the difficulty of solving Maxwell's equations, which form the basis of this analysis, a variety of special

models and techniques have been used, each valid only in a limited range of frequencies or other parameters.

With the availability of improved computer technology, various numerical techniques have been developed for the solution of EMF interactions with objects having irregular geometries and heterogeneous electrical composition. Due to mathematical complexities involved in calculating SAR, a combination of techniques has been used to obtain SAR for various models as functions of frequency. Each of these techniques provides information over a limited range of parameters. Combining the information thus obtained, gives a reasonably good description of SAR as a function of frequency over a wide range of frequencies for a number of useful models.

From a wide array of methods, including the extended-boundary condition method (EBCM) and iterative extended-boundary condition method (IEBCM), method of moments (MOM), finite element method (FEM), finite-element time-domain method (FETD), generalized multipole technique (GMT), the conjugate gradient-fast Fourier transform (CG-FFT), volume-surface integral equation method (VSIE), quasi-static admittance and impedance methods, the FDTD method[33-37] has become the most widely used for bioelectromagnetic applications in the range of a few MHz to several GHz. An extension of the FDTD method, the frequency-dependent finite-difference time-domain method ((FD)^{2}TD)[38, 39], enables broadband bioelectromagnetic simulations by including the effect of the frequency dispersion of the tissues. This method has been used to calculate SAR and current distributions in the body resulting from ultra-short plane wave pulses with bandwidths of the order of 1 GHz.

3.1 Finite-Difference Time-Domain Code

Kunz and Luebbers[33] originally developed an FDTD program to predict SAR distributions in different digital models (sphere, rat, and human). This FDTD code was modified and digital anatomical models were developed jointly by U.S. Naval Health Research Center Detachment and U.S. Air Force Research Laboratory, Brooks City-Base, Texas. The permittivity properties of each of the tissue types are set according to data and approximations published by Gabriel[40]. The modified code reads the anatomical model files and outputs a number of files that include 3-D normalized SAR; mean, minimum, and maximum SARs for each tissue type; and each Z-plane slice. Finally, there is an extensive log file and all file names are automatically constructed to reflect run parameters. The code has been parallelized using the message-passing interface (MPI) library, which allows for larger and more complex data sets to be modeled. The advantage of using the MPI is that the code can run on parallel computer systems composed of networks of computers. In order to run a human model with 1 mm resolution, we had a Linux-based Beowulf parallel processing system with 100 processors and a total of 104 GB of RAM developed (Fig. 7).

The FDTD algorithm was first established by Yee[41] as a three dimensional solution of Maxwell's curl equations:

$$\nabla x E = -\frac{\partial B}{\partial t} = -\mu \frac{\partial H}{\partial t}$$

$$\nabla x H = \sigma E + \varepsilon \frac{\partial E}{\partial t}$$

13

In principle, a volume of space containing any object or collection of objects is subjected to an electromagnetic disturbance, FDTD then solves for the fields throughout the volume as a function of time. The FDTD method was later improved[42-46].

It uses a geometry mesh, usually of rectangular box-shaped cells (voxels), which is readily developed from CT or MRI scans of real human beings or animals. The constitutive parameters for each cell may be set independently so that objects having irregular geometries and heterogeneous electrical composition can be analyzed. The FDTD method has been used for myriad applications including calculating SARs and induced currents in the human body for plane-wave exposures, exposure to leakage fields of parallel-plate dielectric heaters, exposure to pulse EMF, annular phased arrays of aperture and dipole antennas for hyperthermia, coupling of cellular telephones to the head, exposure to RF magnetic fields in magnetic resonance imaging (MRI) machines and exposure to power line fields.

The FDTD method uses simple central-difference approximations to evaluate the space and time derivatives using a time stepping procedure. Inputs are time-sampled analog signals. The region being modeled is represented by two interleaved grids of discrete points. One grid contains the points at which the magnetic field is evaluated. The second grid contains the points at which the electric field is evaluated.

Values of permeability (μ), relative dielectric (ε') and effective conductivity (σ) assigned to each field component in each cell define the position and electrical properties of the scatterer. These parameters can have different values for different field orientations permitting anisotropic materials to be modeled. Their values can also be adjusted at each time-step depending on conditions making it easy to model nonlinear materials. Because the basic elements are cubes, curved surfaces on a scatterer must be "*stair cas*ed". For many configurations this does not present a problem. However for configurations with sharp, acute edges, an adequately stair cased approximation may require a very small grid size. This can significantly increase the computational size of the problem. Surface conforming FDTD techniques with non-rectangular elements have been introduced to combat this problem. One of the more promising of these techniques, which permits each element in the grid to have an arbitrary shape, is referred to as the Finite Volume Time Domain (FVTD) method[44].

As more powerful computers became widely available, use of the FDTD method has increased exponentially[47]. Its use in bioelectromagnetics has been increased as well[48-50]. Unlike the alternatives, the method of moments (MOM)[51] and finite element method (FEM)[52], the FDTD method is scalable, i.e., the CPU time behaves linearly with problem size N. The MOM and FEM methods require matrix inversions (albeit sparse matrices in FEM) and thus scale as N^3. The MOM method is primarily useful for problems with conducting surfaces, but is difficult to apply to permittivity problems of interest here. Its practical limitation is to systems with less than 10^6 cells[53]. The FEM method, with its irregular cell structure, is difficult to parallelize efficiently. The FDTD method with its rectangular cell structure is easy to parallelize, and, in the case of our problem, is compatible with the cellular data formats of the animal and human anatomical models. The main disadvantages of FDTD are object resolution and absorbing boundary conditions (also true in FEM), but sophisticated versions of the FDTD method have been developed to handle these problems[44].

We also have the XFDTD version 6.0 Bio-Pro from Remcom running on dual Pentium III (1 GHz) processors with 4 GB of RAM.
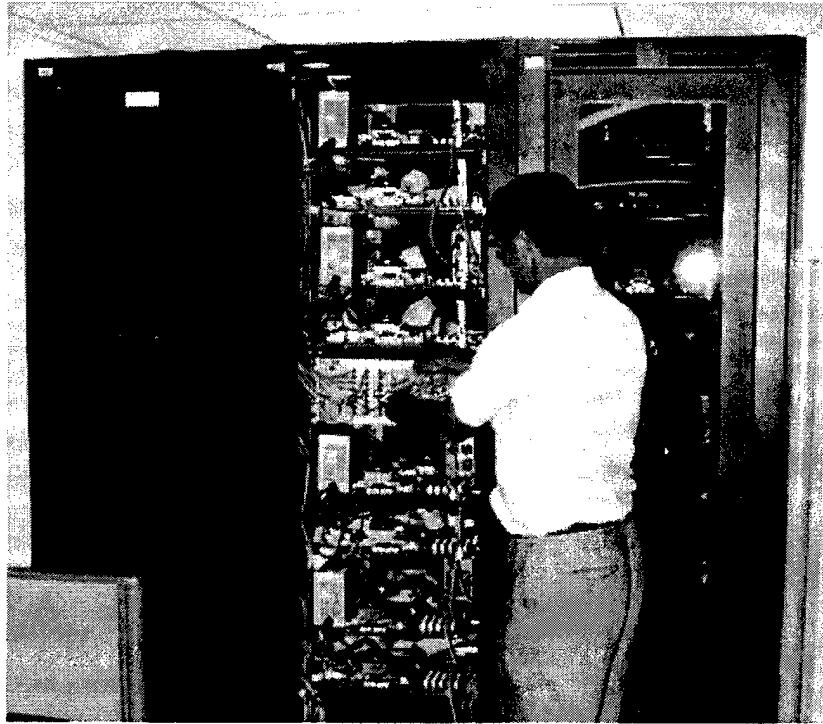

Figure 7. Linux-based Beowulf parallel processing system.

3.2 Models

Over the years, experimental phantoms have been developed to understand coupling of EM fields to models of the biological systems[29]. Early analyses were based on spheres, cylinders, spheroids, ellipsoids, and large-block models (cubical mathematical cells arranged in the shape of a human or animal body). Although these models were relatively crude representations of the size and shape of the human body, experimental results show that calculations of the average SAR agree reasonably well with empirical values[5]. Calculations of the local distribution of the SAR, even though much more difficult, are now becoming possible. Simple homogeneous models have been used[12]. Though these simplistic models are incapable of giving accurate SAR distributions, they do allow use of actual near-field sources such as wireless telephones. And, they have been shown to give peak 1-g SARs needed for SAR compliance testing within an uncertainty of ± 20 %[12, 54].

Concomitant with the development of homogeneous models, the resolution of heterogeneous anatomically based models of the human body has been increasing. Initially based on anatomical sectional diagrams, more recent versions are based on MRI scans of living humans[55-57] or cadavers such as "visible man" and "visible woman" developed by National Library of Medicine[18](See Fig. 9). Development of models suitable for FDTD dosimetric calculations, while straightforward, is not trivial. MRI and CT scans provide

15

voxel maps of density, but many of the tissues have the same or similar densities, and many of the regions outside of the major organs require a detailed understanding of anatomy to determine what tissues are present, e.g., fat, muscle, bone. Even when some automatic tissue definition can be used, the bulk of the task falls on manual tissue recognition by a trained anatomist. Moreover, since FDTD calculations use the tissue electrical properties, i.e., dielectric value and conductivity, and mass density at each voxel location, knowledge of these properties for each cell is also required. With the advent of larger memory in PCs, computer workstations, and parallel processors, it is possible to run anatomically based whole-body models with resolutions on the order of a millimeter and even sub-millimeter resolution models for partial body exposures (e.g. head and neck) for exposures such as wireless telephones[58]. Anatomically based models of the common laboratory animals such as the rat, goat, and rhesus monkey have also been developed[59] and used for dosimetric calculations because of the importance of such subjects for laboratory experiments[60, 61].

Development of the anatomical models of the Sprague-Dawley rat and man has been described in details[18, 58]. Briefly, magnetic resonance imaging (MRI) was used to acquire axial scans of the rat. Images of the man were obtained from the Visible Human project (National Library of Medicine). Initial computer-segmentation of tissue types on the man images was completed by CieMed (a collaboration between National University of Singapore and Johns Hopkins University). The original x, y, z voxel dimensions were .39 x .39 x 3.0 mm for the rat and 1.0 x 1.0 x 1.0 mm for the man. Each voxel was color-coded and assigned a tissue type. In addition to these models, we have produced computer anatomical models of a rhesus monkey, phantom monkey, pigmy goat, and rat (Fig. 8). These models are available via anonymous FTP from starview.brooks.af.mil/EMF.
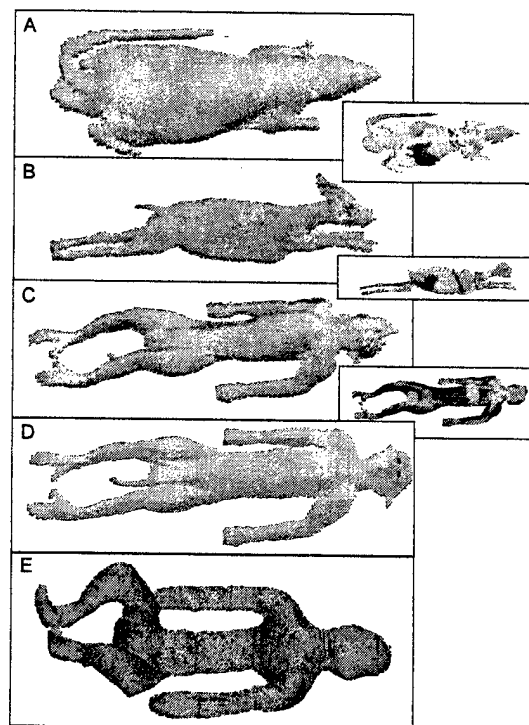

Figure 8. Models of A) Rat, B) Goat, C & D) Monkey, and E) Phantom Monkey.
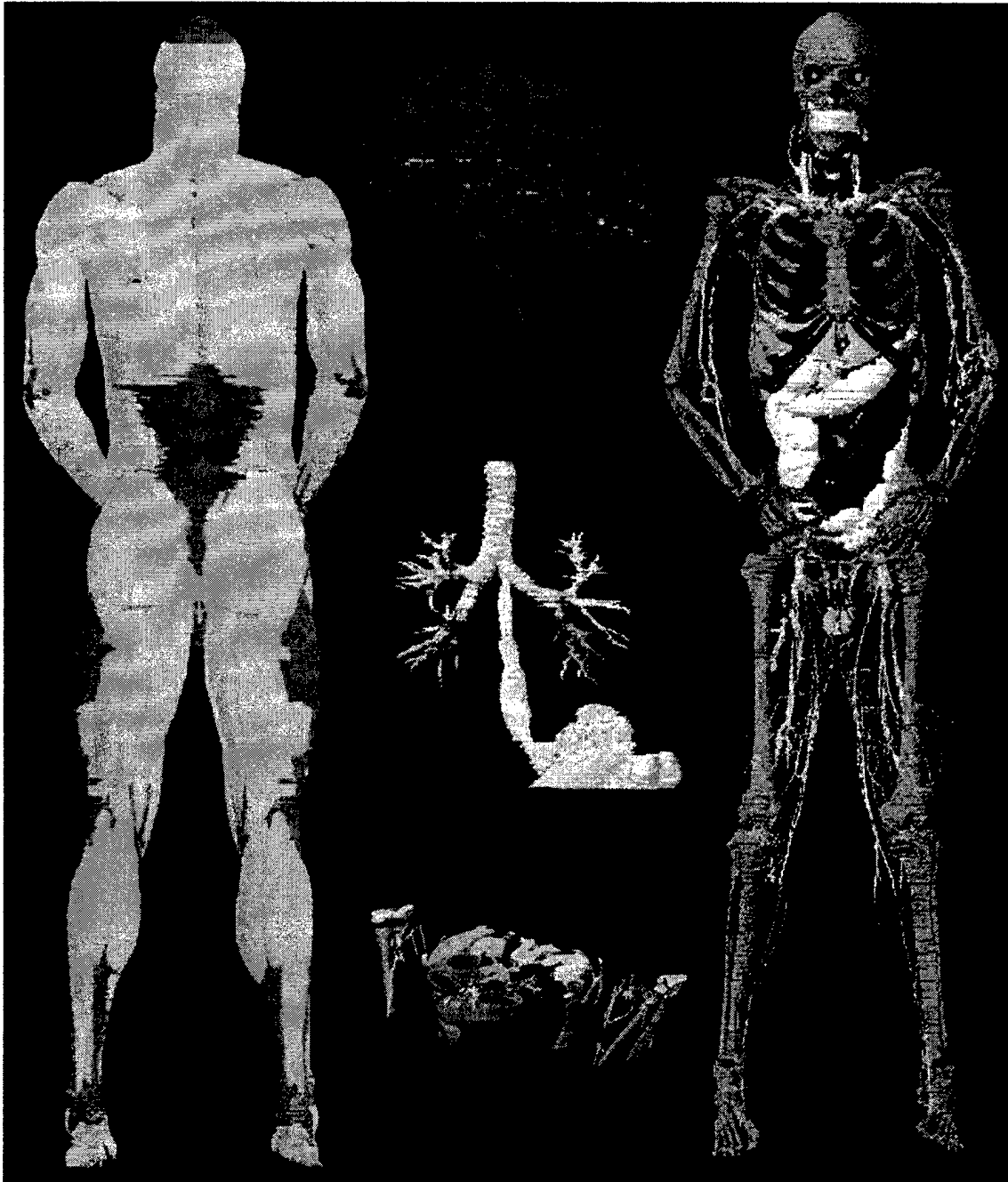
16

Figure 9. Visible Man Model

We also are running Varipose from Remcom which allows us to reposition the visible human mesh. This software was developed through the AFRL-sponsored Small Business Innovative Research program.

Prof. Deborah Silver with the Center for Advanced Information Processing, Rutgers University, is developing software for repositioning the animal models.

3.3 Electrical Properties

Determining permittivity values (ε' and σ) of various biological tissues is a critical step when calculating the SAR. However, various authors[40, 62-66] report different permittivity values for the same tissue type. This lack of consensus on which permittivity values represent the most accurate values of the biological tissues poses the question of the effect of permittivity value on calculated SAR values in biological systems. Since there is some variability in the tissue permittivity values of human and animals and some uncertainty in the measurement of the permittivity of tissues, the dependence of SAR on permittivity changes is important[67].

The most recent and comprehensive permittivity data set includes[40] more than 30 tissue types in the frequency range 10 Hz to 20 GHz and on more than 20 other types from 10 MHz to 20 GHz. Three main interaction mechanisms, each governed by its own kinetics, determine the main features of the permittivity spectrum of a biological tissue. Three main spectral regions known as the α, β and γ dispersions are predicted from known interaction mechanisms (Fig. 10). These dispersions have been identified experimentally in the frequency range from hertz to gigahertz. The γ dispersion, in the gigahertz region, is due to the polarization of water molecules. The β dispersion, typically in the hundreds of kilohertz region, is due mainly to the polarization of cellular membranes that act as barriers to the flow of ions between the intra- and extracellular media. Other contributions to the β dispersion come from the polarization of protein and other organic macromolecules. The low frequency α dispersion is associated with ionic diffusion processes at the site of the cellular membrane[68].
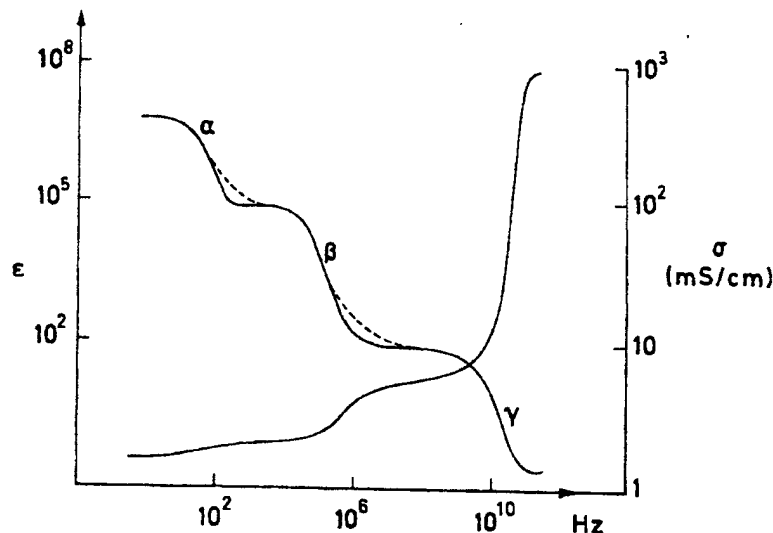
Figure 10. Dielectric value (ε') and conductivity (σ in mS/m) of the muscle are shown as a function of frequency[69]. Three major dispersion α, β, and γ are typical for all tissues and cells in suspension, although magnitudes and dispersion frequencies vary. Additionally smaller relaxation effects contribute to the high frequency –tails of α and β dispersions, as indicated by the dashed curves.

We use an HP 8510 Network Analyzer (Fig. 11) to measure the reflection coefficient from an open ended coaxial probe that is in contact with the material of interest (biological tissue or liquid media). These reflection coefficient values are then used to calculate the electrical properties (permittivity) of this material[40]. Measurements can be performed for frequencies from 45 MHz to 26.5 GHz.
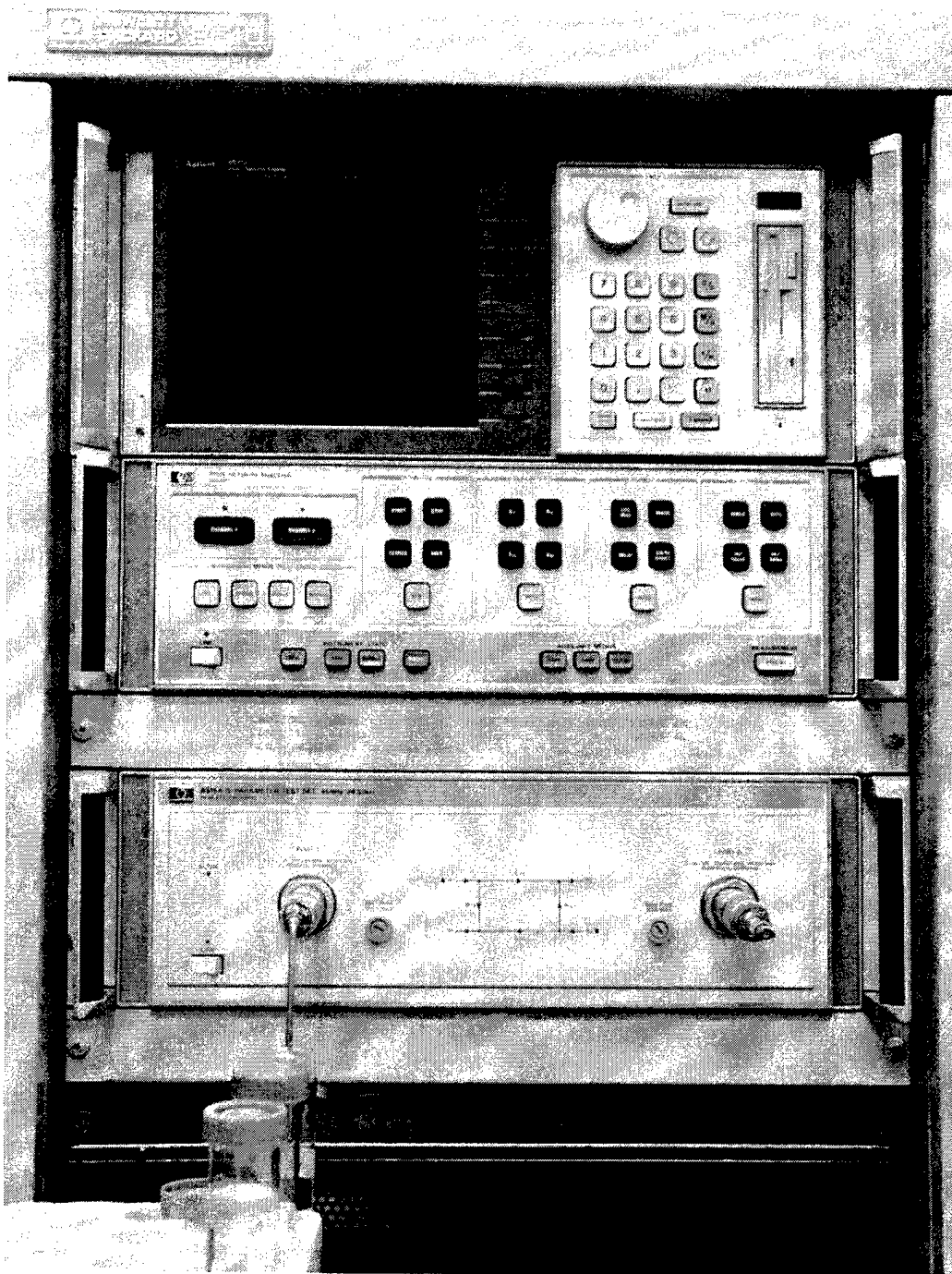

Figure 11. HP 8510 Network Analyzer

4.0 <u>INTERNATIONAL EMF DOSIMETRY HANDBOOK</u>

The 5th Edition of the Radio Frequency Dosimetry Handbook (RFDH) will expand on the 4th Edition by updating RF dosimetry research that has been accomplished since 1986, primarily in the fields of localized specific absorption rate (SAR) and temperature distribution resulting from exposure to RF fields. The 5th Edition will have approximately two dozen chapters included under the broad categories of general RF principles, computational modeling, analytical/empirical dosimetry, experimental dosimetry, and exposure assessment. Dr. E. Adair will be writing the chapter on Thermal Responses to RF Exposure, Prof. M. Ziskin on Responses to RF Overexposure, S.Allen on Empirical RF Dosimetry Techniques, W. Hurt on Basics of Electromagnetics, and Dr. J. Leonowich on Personal Dosimetry Indicators. We will contact about six other experts to write additional chapters. Dr. P. Chadwick, Microwave Consultants Limited, England, is negotiating with other experts to write approximately 14 chapters as well. The projected schedule calls for the authors to submit their chapters in draft form starting in 2003.

5.0 <u>SUMMARY</u>

Knowledge of internal electric and magnetic fields, induced current densities, and SARs is of basic interest in the assessment of biological effects and medical applications of electromagnetic fields. Dosimetry is an important part of any scientific effort to assess the effects of EMF on biological organisms. Experimental dosimetry is essential in determining the internal fields and the whole body or localized SAR values in experiments with phantoms or animals. Furthermore, carefully performed experiments are crucial in verification of theoretical predictions and delineation of their limitations. In the last few years, considerable progress has been achieved in experimental and numerical dosimetry. Today a broad range of tools for dosimetric analysis for the wide frequency range is available. Because of the heterogeneity of the tissues and the nonuniformity of the incident fields, closed-form analytical solutions are impossible and computer methods are needed to obtain the internally coupled fields. In theoretical dosimetry, FDTD is currently the most acceptable choice if digital anatomical models of man and animals (highly inhomogeneous structures of millimeter resolution) are to be analyzed. The main contribution of our research efforts to the discipline of theoretical dosimetry is identification of the dependence of predicted SAR in relation to the variability in permittivity values for different tissue types (muscle, fat, skin, bone marrow) when using different numerical anatomical models. Whole body SAR is not particular sensitive to variations in permittivity values, while localized SAR values have a great dependence on them. The ratios in whole body and localized SAR values are also dependent on different exposure conditions (orientation, frequency).

6.0 REFERENCES

1. Gajšek P: Radiofrequency Measurements and Sources, In Klauenberg BJ and Miklavcic D, (eds.) "Radio Frequency Radiation Dosimetry and Its Relationship to the Biological Effects of Electromagnetic Fields." Kluwer Academic Publishers B.V., Dordrecht, The Netherlands, pp. 309-320 (2000).

2. D'Andrea JA, Gandhi OP, and Lords JL: Behavioral and thermal effects of microwave radiation at resonant and nonresonant wavelengths. Radio Science, vol. 12(6S), pp. 251-256 (1977).

3. D'Andrea JA, Emmerson RY, Bailey CM, Olsen RG, and Gandhi OP: Microwave radiation absorption in the rat: Frequency-dependent SAR distribution in body and tail, Bioelectromagnetics, vol. 6: pp. 199-206 (1985).

4. Gandhi OP, Hagmann MJ, and D'Andrea JA: Partbody and multibody effects on absorption of radio frequency electromagnetic energy by animals and by models of man. Radio Science, vol. 14(6S): pp. 15-22 (1979).

5. Durney CH, Massoudi H, and Iskander MF: Radiofrequency Radiation Dosimetry Handbook (Fourth Edition), USAFSAM-TR-85-73, USAF School of Aerospace Medicine, Brooks Air Force Base, TX 78235 (1986).

6. Gandhi OP: Polarization and frequency effects on whole animal energy absorption of RF energy. Proc. IEEE, vol. 62, pp. 1171-1175 (1974).

7. Hurt WD: Dosimetry of radiofrequency (RF) fields, in K. Hardy, M. Meltz, and R. Glickman (eds.), Non-Ionizing Radiation: An Overview of the Physics and Biology, Health Physics Society 1997 Summer School, Medical Physics Publishing, Madison, Wisconsin (1997).

8. Mason PA, Hurt WD, Walters TJ, D'Andrea JA, Gajšek P, Ryan KL, Nelson PA, and Ziriax JA: Effects of frequency, permittivity, and voxel size on predicted specific absorption rate values in biological tissue during electromagnetic field exposure, IEEE Trans. Microwave Theory Tech., vol. MTT-48, no. 11, pp. 2050-2057 (2000).

9. Kritikos HN and Schwan HP: Hot spots generated in conducting spheres by electromagnetic waves and biological implications, IEEE Trans. Biomedical Eng., vol. 19 (1), pp. 53-58 (1972).

10. Kritikos HN and Schwan HP: The distribution of heating potential inside lossy sphere, IEEE Trans. Biomedical Eng., vol. BME-22 (6), pp. 457-463 (1975).

11. Ohlsson T and Risman PO: Temperature distribution of microwave heating – spheres in cylinders, J. Microw. Power, vol. 13 (4), pp. 303-310 (1978).

12. Gandhi OP, Lazzi G, Tinniswood A, and Yu Q: Comparison of numerical and experimental Methods for determination of SAR and Radiation patterns of Handheld Wireless Telephones, Bioelectromagnetics, vol. 20, pp. 93-101 (1999).

13. Mie G: Contributions to the optics of diffusing media. Ann Physik, vol. 25(1908).

14. Walters TJ, Mason PA, Ryan KL, Nelson DA, and Hurt WD: A comparison of SAR values determined empirically and by FDTD modeling, In Klauenberg BJ and Miklavcic D, (eds.) "Radio Frequency Radiation Dosimetry and Its Relationship to the Biological Effects of Electromagnetic Fields." Kluwer Academic Publishers, B.V. Dordrecht, The Netherlands, pp. 207-216 (2000).

15. Chou CK, Bassen H, Osepchuck J, Balzano Q, Peterson R, Meltz M, Cleveland R, Lin JC, and Heynick L: Radio frequency electromagnetic exposure: Tutorial review on experimental dosimetry, Bioelectromagnetics, vol. 17, pp. 341-353 (1996).

16. Greene FM: Development of Electric and Magnetic Near-Field Probes, NBS Technical Note 658, U.S. Department of Commerce, National Bureau of Standards, Boulder, Colorado (1975).

17. National Council on Radiation Protection and Measurements (NCRP): A Practical Guide to the determination of Human Exposure to Radiofrequency Fields, Report 119 (1993).

18. Mason PA, Ziriax JM, Hurt WD, Walters TJ, Ryan KL, Nelson PA, and. D'Andrea JA: "Recent advances in dosimetry and modeling", In Klauenberg BJ and Miklavcic D, (eds.): Radio Frequency Radiation Dosimetry and Its Relationship to the Biological Effects of Electromagnetic Fields, Kluwer Academic Publishers B.V., Dordrecht, The Netherlands, pp. 141-155 (2000).

19. Kuster N, Balzano Q, and Lin JC: Mobile Communication Safety, First Edition, Chapman & Hall (1997).

20. Allen SJ and Hurt WD: Calorimetric measurement of microwave energy absorption in mice after simultaneous exposure of 18 animals, Radio Science, vol. 14, pp. 1-4 (1979).

21. Blackman CF and Black JA: Measurement of microwave radiation absorbed in biological systems, 2, analysis of Dewar-flask calorimetry, Radio Science, vol. 12, pp. 9-14 (1977).

22. Olsen RG and Griner TA: Outdoor measurements of SAR in a full-size human model exposed to 29.2 MHz near-field irradiation, Bioelectromagnetics, vol. 10, pp. 162-171 (1989).

23. Padilla JP and Bixby R: Using Dewar-Flask Calorimetry and Rectal Temperatures to Determine the Specific Absorption Rates of Small Rodents. USAF School of Aerospace Medicine Report, USAFSAM-TP-86-3, Brooks AFB, TX (1986).

24. Hochuli C: Procedures for Evaluating Nonperturbing Temperature Probes in Microwave Fields, FDA 81-8143, Food and Drug Administration, Rockville, MD 20857 (1981).

25. Bowman RR: A Probe for Measuring Temperature in Radio-Frequency Heated Material. IEEE Trans. Microwave Theory Tech., vol. MTT-24, p. 43 (1976).

26. Smolenski DM: Evaluation of Analog Interface for Dosimetry Temperature Probes. USAF Armstrong Laboratory Report, AL/OE-TR-1996-0141, Brooks AFB, TX (1996).

27. Guy AW: Dosimetry associated with exposure to non-ionizing radiation: very low frequency to microwaves, Health Phys., vol. 53, no. 6, pp. 569-584 (1987).

28. Walters TJ, Blick DW, Johnson LR, Adair ER, and Foster KR: Heating and pain sensation produced in human skin by millimeter waves. Health Phys., vol. 78, no.3, pp. 259-267 (2000).

29. Stuchly MA and Stuchly SS: Experimental radiowave and microwave dosimetry, in C. Polk and E. Postow (eds.) Handbook of Biological Effects of Electromagnetic Fields, Second Edition, CRC Press Inc., Boca Raton, FL, pp. 301-342 (1996).

30. Bassen HI, Herchenroeder P, Cheung A, and Neuder SM: Evaluation of implantable electric field probes within finite simulated tissues, Radio Science, vol. 12, pp. 15-23 (1977).

31. Christman CL, Ho HS, and Yarrows S: "A Microwave Dosimetry System for Measured Sampled Integral-dose Rate," IEEE Trans. Microwave Theory Tech., vol. MTT-22, no. 12, pp. 1267-1278 (1974).

32. Ho HS and Edwards WP: "Oxygen-consumption Rate of Mice under Differing Dose Rates of Microwave Radiation," Radio Science, vol. 12, no. 6(S), pp. 131-138 1977.

33. Kunz KS and Luebbers RJ: The Finite Difference Time Domain Method for Electromagnetics, CRC Press, Inc., Boca Raton, Florida (1993).

34. Chen J Y, Gandhi OP, and Conover DL: SAR and Induced Current Distributions for Operator Exposure to RF Dielectric Sealers," IEEE Trans. Electromagnetic Compatibility, vol. EMC-33, no. 3, pp. 252-261 (1991).

35. Gandhi OP: Numerical Methods for Specific Absorption rate Calculations," Chapter 6 in Biological Effects and Medical Applications of Electromagnetic Energy, O.P. Gandhi Ed., pp. 113-140, Prentice Hall, Englewood Cliffs, New Jersey (1990).

36. Lin JC and Gandhi OP: Computational methods for predicting field, in C. Polk, an E Postow (eds) Biological Effects of Electromagnetic Fields, 2nd Edition, CRC Press Inc., Boca Raton, FL, pp.337-402 (1996).

37. Taflove A: "Computational Electrodynamics – The Finite-Difference Time-Domain Method", Artech House, Boston (1995).

38. Luebbers R, Hunsberger FP, Kunz KS, Sandler RB, and Schneider M: A Frequency-Dependent Finite-Difference Time-Domain Formulation for Dispersive Materials," IEEE Trans. Electromagnetic Compatibility, vol. EMC-32, pp. 222-227 (1990).

39. Sullivan DM: Frequency-Dependent FDTD Methods using Z Transformations, IEEE Trans. Antennas and Propagation, vol. AP-40, pp. 1232-1230 (1992).

40. Gabriel C: Compilation of the Dielectric Properties of Body Tissues at RF and Microwave Frequencies, AL/OE-TR-1996-0037, Armstrong Laboratory, Brooks Air Force Base, TX 78235 (1996).

41. Yee KS: Numerical solution of initial boundary value problems involving Maxwell's equations in isotropic media. IEEE Trans. Antennas and Propagation, vol. AP-14, p. 302 (1966).

42. Taflove A and Brodwin ME: Computation of the electromagnetic fields and induced temperatures within a model of the microwave irradiated human eye, IEEE Trans. Microwave Theory Tech., vol. MTT-23, p. 888 (1975).

43. Taflove A and Brodwin ME: Numerical Solutions of Steady-State Electromagnetic Scattering Problems using the Time-Dependent Maxwell's Equations, IEEE Trans. Microwave Theory Tech., vol. MTT-23, pp. 623-630 (1975).

44. Taflove A: "Computational Electrodynamics – The Finite-Difference Time-Domain Method", Artech House, Boston (1995).

45. Holland R: THREDE: a free-field EMP coupling and scattering code, IEEE Trans. Nuclear Science, vol. NC-24, pp. 2416-2421 (1977).

46. Kunz KS and Lee KM: A three-dimensional finite-difference solution of the external response of an aircraft to a complex transient EM environment, 1. The method and it's implementation. IEEE Trans. Electromagnetic Compatibility, vol. EMC-20, p. 328 (1978).

47. Shlager KL and Schneider JB: A Selective Survey of the Finite-Difference Time-Domain Literature. IEEE Antennas and Propagation Magazine, vol. 37, no. 4, pp. 39-56 (1995).

48. Gandhi OP: Some Numerical Methods for Dosimetry: ELF to microwave frequencies. Radio Science, vol. 29, pp. 12-19 (1994).

49. Stuchly MA and Gandhi OP: Interlaboratory comparison of the numerical dosimetry for human exposure to 60 Hz electric and magnetic fields, Bioelectromagnetics, vol. 21, pp. 167-174 (2000).

50. Dimbylow PJ: FDTD calculations of the whole-body averaged SAR in an anatomically realistic voxel model of the human body from 1 MHz to 1 GHz. Physics in Medicine and Biology, vol. 42, pp. 479-490 (1997).

51. Harrington RF: "Field Computation by Moments Method", The Macmillan Company, New York (1968).

52. MacNeal BE: MSC/EMAS Modeling Guide, The MacNeal-Schwendler Corporation (1991).

53. Ziriax JH, Jennings JK, D'Andrea JA, Mason PA, Halftel M, and Hurt WD: Using the visible human data set for FDTD calculations, In: Millenium Workshop on Biological Effects of EMF, Proceedings (Eds: Kostarakis, Stavroulakis), pp. 62-72 (2000).

54. Taylor CH, Burl M, and Hand WJ: Experimental verification of numerical predicted electric field distributions produced by a radiofrequency coil, Phys. Med. Biol., vol. 42, pp. 1395-1402 (1997).

55. Gandhi OP: Some numerical methods for dosimetry: Extremely low frequencies to microwave frequencies, Radio Science, vol. 30, pp. 161-177 (1995).

56. Dimbylow PJ: Development of realistic voxel phantoms for electromagnetic field dosimetry, 1-7, in P. J. Dimbylow (ed.) Voxel Phantom Development, Proceedings of an International Workshop, National Radiological Protection Board, Chilton, Didcot, U.K (1996).

57. Zubal IG, Harrell CR, Smith EO, Rattner Z, Gindi GR, and Hoffer PH: Computerized three-dimensional segmented human anatomy, Med. Phys. Biol., vol. 21, pp. 299-302 (1994).

58. Tinniswood AD, Furse CM, and Gandhi OP: Computations of SAR distributions for two anatomically-based models of the human head using CAD files of commercial telephones and the parallelized FDTD code, IEEE Trans. Antennas and Propagation, vol. AP-46, pp. 829-833 (1998).

59. Mason PA, Walters TJ, Fanton JW, Erwin DN, Gao JH, Roby JW, Kane JL,. Lott, KA and Blystone RV: Database created from magnetic resonance images of a Sprague-Dawley rat, rhesus monkey, and pigmy goat, Official Publication of the Federation of American Societies for Experimental Biology (FASEB J.), vol. 9, pp. 434-440 (1995).

60. Tinniswood AD and Gandhi OP: Head and neck resonance in a rhesus monkey -- A comparison with results from a human model, Physics in Medicine and Biology, vol. 44, pp. 695-704 (1999).

61. Tinniswood AD, Furse CM, and Gandhi OP: Power deposition in the head and neck of an anatomically-based human body model for plane wave exposures, Physics in Medicine and Biology, vol. 43, pp. 2361-2378 (1998).

62. Gabriel C, Gabriel S, and Corhout E: The Dielectric Properties of Biological Tissues: Literature Survey, Physics in Medicine and Biology, vol. 41, pp. 2231-2249 (1996).

63. Schwan HP: Electrical properties of tissues and cells, Advan. Biol. Med. Phys., vol. 5, pp. 147-209 (1957).

64. Schwan HP: Electrical properties of phospholipid vesicles, Biophys. J., vol. 10, pp. 1102–1119 (1970).

65. Stuchly MA and Stuchly SS: Dielectric properties of biological substances – Tabulated, J. Microwave Power, vol. 15, pp. 19–26 (1980).

66. Duck FA: Physical Properties of Tissue – A Comprehensive Reference Book, Academic Press (1993).

26

67. Hurt WD, Ziriax JM, and Mason PA: Variability in EMF permittivity values: Implications for SAR calculations, IEEE Trans. Biomed. Eng., vol. BME-47, no. 3, pp. 396-401 (2000).

68. Foster KR and Schwan HP: Dielectric Properties of Tissues, In: Polk C, Postow E (eds): Handbook of Biological effects of Electromagnetic Fields, second edition, CRC Press (1996).

69. Schawn HP: Dielectric Properties of Biological Materials and Interaction of Microwave Fields at the Cellular and Molecular Level. In SM Michaelxon and MW Miller (eds.). Fundamental and Applied Aspects of Nonionizing Radiation. New York: Plenum Publishing Co. (1975).

70. Steinhart JS and Hart SR: Deep-Sea Research, vol. 15, p. 497 (1968).